

## Highly Potent Inhibitors of Methionine Aminopeptidase-2 Based on a 1,2,4-Triazole Pharmacophore<sup>†</sup>

Joseph P. Marino, Jr.,\* Paul W. Fisher,<sup>‡</sup> Glenn A. Hofmann, Robert B. Kirkpatrick, Cheryl A. Janson,<sup>§</sup> Randall K. Johnson,<sup>||</sup> Chun Ma,<sup>⊥</sup> Michael Mattern,<sup>#</sup> Thomas D. Meek, M. Dominic Ryan,<sup>⊗</sup> Christina Schulz, Ward W. Smith,<sup>○</sup> David G. Tew, Thaddeus A. Tomazek, Jr., Daniel F. Veber,<sup>□</sup> Wenfang C. Xiong,<sup>◇</sup> Yuuichi Yamamoto, Keizo Yamashita, Guang Yang,<sup>◆</sup> and Scott K. Thompson

Departments of Medicinal Chemistry, Enzymology, Oncology, and Structural Biology, GlaxoSmithkline, King of Prussia, Pennsylvania 19406

Received October 11, 2006

High-throughput screening for inhibitors of the human metalloprotease, methionine aminopeptidase-2 (MetAP2), identified a potent class of 3-anilino-5-benzylthio-1,2,4-triazole compounds. Efficient array and iterative synthesis of triazoles led to rapid SAR development around the aniline, benzylthio, and triazole moieties. Evaluation of these analogs in a human MetAP2 enzyme assay led to the identification of several inhibitors with potencies in the 50–100 picomolar range. The deleterious effects on inhibitor potency by methylation of the anilino-triazole nitrogens, as well as the X-ray crystal structure of triazole **102** bound in the active site of MetAP2, confirm the key interactions between the triazole nitrogens, the active site cobalt atoms, and the His-231 side-chain. The structure has also provided a rationale for interpreting SAR within the triazole series. Key aniline (2-isopropylphenyl) and sulfur substituents (furanylmethyl) identified in the SAR studies led to the identification of potent inhibitors (**103** and **104**) of endothelial cell proliferation. Triazoles **103** and **104** also exhibited dose-dependent activity in an aortic ring tissue model of angiogenesis highlighting the potential utility of MetAP2 inhibitors as anticancer agents.

### Introduction

Angiogenesis is a key process in the progression of a number of diseases such as diabetic retinopathy, rheumatoid arthritis, and cancer.<sup>1</sup> In the cancer area, it has been demonstrated that tumors cannot metastasize without the formation of new blood vessels.<sup>1</sup> Biological transformations and pathways that play a role in angiogenesis are, therefore, particularly attractive targets as potential methods for inhibiting solid tumor growth/metastasis. Methionine aminopeptidase type 2 (MetAP2<sup>a</sup>) has been identified as the intracellular target for the potent antiangiogenesis agent fumagillin (**1**; Figure 1), a natural product from *Aspergillus fumigatus*.<sup>3</sup> Early drug discovery efforts have focused on analogs of fumagillin, which irreversibly inhibit MetAP2 through covalent modification of an epoxide. Fumagillin analogs such as **2a** (TNP-470; Figure 1) and **2b** (PPI-2458; Figure 1), potent selective inhibitors of MetAP2 proteolytic activity and endothelial cell proliferation, have been in clinical trials for the treatment of a variety of tumors.<sup>4</sup> Only recently

have reversible human MetAP2 inhibitors been reported, many of which possess structures derived from peptides.<sup>5</sup> There are very few examples of metalloprotease or MetAP2 inhibitors that rely on key binding interactions between a heterocycle and active-site metal ions, along with amino acid residues.<sup>7</sup> In this paper, we disclose an anilino-1,2,4-triazole class of heterocyclic metalloprotease inhibitors, detailing the array and iterative synthesis of these compounds as well as key structural activity relationships. X-ray crystallographic studies are reported that reveal key binding interactions between the heterocycle and the enzyme. Several compounds were found to be potent inhibitors of endothelial cell proliferation and also showed promising activity in an angiogenesis assay.

### Synthesis

High-throughput screening (GSK compound collection) of the cobaltous form of methionine aminopeptidase-2 led to the discovery of triazole inhibitor **6**. In an effort to follow up on this hit, we investigated two efficient synthetic routes for the preparation of 3-anilino-5-benzylthio-1,2,4-triazoles. The first strategy was developed by Kurzer and Douraghi-Zadeh<sup>8</sup> and is initiated by the *S*-benzylation of acetone thiosemicarbazone (**3**) followed by treatment of the resulting acetone *S*-benzylisothiosemicarbazone with diphenylcarbodiimide (Scheme 1). Exposure of the *N,N'*-diarylamidine product (**5**) to acid led to cyclization, affording the target molecule **6** in good yield with concomitant expulsion of acetone and aniline. Although this route is short, it was clear that a diverse set of anilino-triazoles could not be synthesized using this approach because the commercial availability of substituted diphenylcarbodiimides was limited.

The second approach undertaken, first discovered by Davidson,<sup>9</sup> was found to be more readily amenable to rapid analoging. Davidson found that nucleophilic attack on isobiuret **9** by hydrazine led to the displacement of ethanethiol, followed by cyclization of the amino group of the guanidine onto the

<sup>†</sup> Coordinates and structure factor files for methionine aminopeptidase-2 complexed to **102** have been deposited in the Protein Data Bank under the access code 2OAZ.

\* To whom correspondence should be addressed. Phone: (610)-270-5496. Fax: (610)-270-4490. E-mail: joseph.p.marino@gsk.com.

<sup>‡</sup> Current address: Centocor, Inc., Radnor PA.

<sup>§</sup> Current address: Shamrock Structures, Woodridge, IL.

<sup>||</sup> Current address: Independent consultant, Santa Fe, NM.

<sup>⊥</sup> Current address: Hoffman-La Roche, Inc., Nutley, NJ.

<sup>#</sup> Current address: Progenra, Inc., Malvern, PA.

<sup>⊗</sup> Current address: Millennium Pharmaceuticals, Cambridge, MA.

<sup>○</sup> Current address: Argonne National Laboratory, Argonne, IL.

<sup>□</sup> Current address: Independent consultant, Ambler, PA.

<sup>◇</sup> Current address: Finnegan Henderson, Palo Alto, CA.

<sup>◆</sup> Current address: Tanabe Research Laboratories U.S.A., Inc., San Diego, CA.

<sup>a</sup> Abbreviations: MetAP2, methionine aminopeptidase type 2; MetAP1, methionine aminopeptidase type 1; HUVEC, human umbilical vein endothelial cell; MS-1, murine stroma cell type 1; XTT, cell growth inhibition assay employing 2,3-bis(2-methoxy-4-nitro-5-sulfophenyl)-5-[(phenylamino)carbonyl]-2H-tetrazolium hydroxide sodium salt.

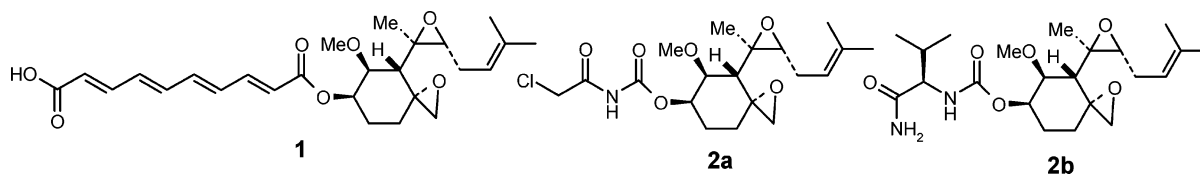
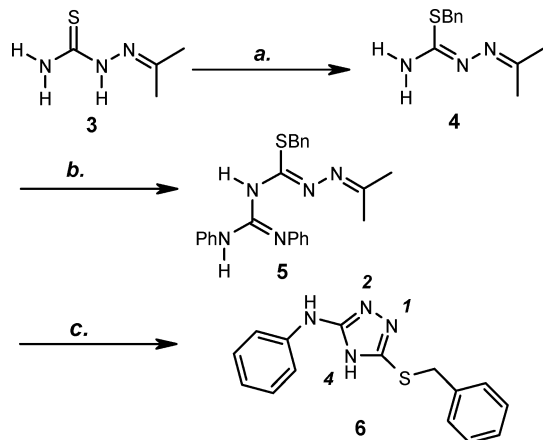


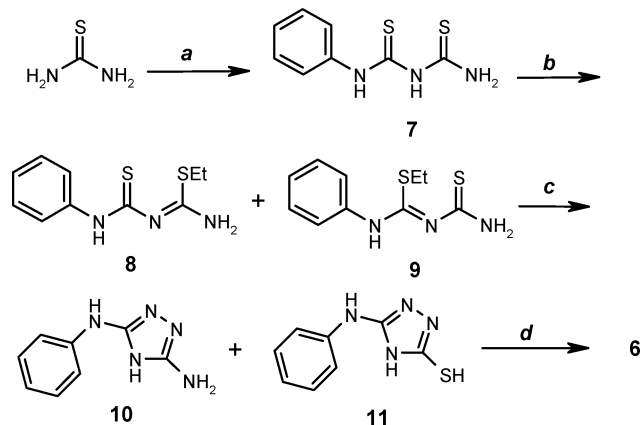
**Figure 1.** Irreversible inhibitors of methionine aminopeptidase-2.

**Scheme 1.** Kurzer and Douraghi Method<sup>a</sup>



<sup>a</sup> Reagents and conditions: (a) BnCl, NaOH, EtOH, 60%; (b) diphenylcarbodiimide, acetone, reflux, 40%; (c) 10% HCl (EtOH), 70%.

**Scheme 2.** Davidson Method via Thiourea<sup>a</sup>



<sup>a</sup> Reagents and conditions: (a) phenylisothiocyanate, NaOH, H<sub>2</sub>O, CH<sub>3</sub>CN 60%; (b) EtI, Et<sub>3</sub>N, DMF, 70%; (c) NH<sub>2</sub>NH<sub>2</sub>, EtOH, 80 °C, 60%; (d) BnBr, K<sub>2</sub>CO<sub>3</sub>, DMF, 80%.

thiourea (Scheme 2). Aromatization of the triazole ring through the loss of ammonia afforded the mercapto-triazole **11** in 70% yield. The diaminotriazole product **10** was also formed as a minor product (20%), however, **11** could be selectively precipitated by trituration of the crude reaction mixture with aqueous HCl. Since an efficient synthesis of isobiuret **9** had not been reported in the literature, a sequence was developed which utilized common synthetic building blocks. The synthesis of the key biuret intermediate **7** and the triazole **6** is summarized in Scheme 2. In the first step, thiourea is reacted with phenylisothiocyanate<sup>10</sup> in aqueous sodium hydroxide to produce 1-phenyldithiobiuret **7**. The biuret **7** was treated with ethyl iodide in the presence of triethylamine to give a 2:1 mixture of a *S*-alkylation products **8** (minor) and **9** (major), which were separable by column chromatography. Heating the isobiuret **9** in ethanol in the presence of hydrazine hydrate afforded the cyclization product **11**. Mercapto-triazole **11** was then selectively alkylated with one equivalent of benzyl bromide in the presence

of potassium carbonate to afford the 1,2,4-triazole **6** in good yield. Because a wide diversity of arylisothiocyanates and benzyl bromides were commercially available, the chemistry was ideal for two-dimensional parallel array synthesis.

To explore the SAR around the aniline group of the 1,2,4-triazole **6**, eight substituted phenyl-isothiocyanates were selected that contained both electron-rich and electron-poor aromatic substituents. The requisite eight mercapto-triazoles were obtained via the Davidson synthesis, and the resulting thiols were then treated with twelve alkyl halides in the presence of potassium carbonate to provide the desired triazole targets. Alkylation reactions of the eight mercaptotriazoles (employing 12 commercially available alkyl-halides) were carried out in a 96-well plate. Automated liquid handling instrumentation facilitated filtration and liquid transfer. A total of 83 compounds out of a possible 96 were successfully synthesized (highlighted in Table 1). Yields ranged from 50% to 90%, with greater than 95% purity after reverse phase HPLC purification.

To determine the importance of the heterocyclic and aniline nitrogens for binding, a series of *N*-methylated triazoles were synthesized, as shown in Scheme 3. Treatment of **6** with sodium hydride led to deprotonation of the more acidic heterocyclic protons. Addition of methyl iodide led to the formation of two products in which alkylation had occurred on nitrogens **2** and **1** of the triazole ring to provide a 1:1 mixture of *N*-methyl-triazoles **95** and **96**, respectively (Scheme 3). Regiochemistry was unambiguously established by heteronuclear correlations and NOE (based on the position of the methyl group in relation to the aniline proton). Following a protecting group strategy commonly used for imidazole rings,<sup>11</sup> the triazole ring was readily alkylated with chloromethyl ethyl ether and protected as the ethoxymethyl ether. The aniline nitrogen was methylated by treatment with sodium hydride and iodomethane in DMF and subsequently deprotected with trifluoroacetic acid to afford the *N*-Me-aniline **98**.<sup>12</sup>

### Biological Activity

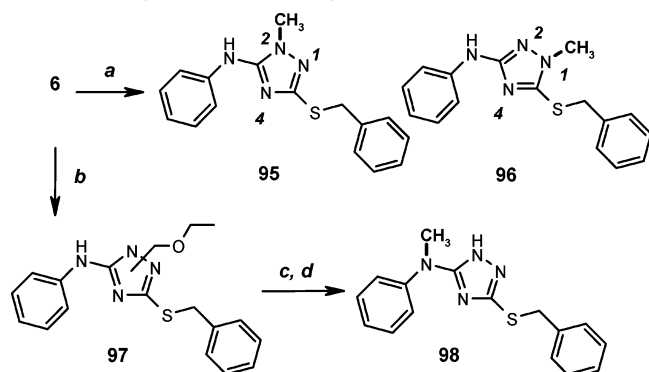
In addition to the discovery that 1,2,4-triazole **6** was a potent inhibitor ( $K_{i,app} = 0.5$  nM) of the Co<sup>2+</sup>-MetAP2 enzyme, it was also found to be quite selective versus Co<sup>2+</sup>-MetAP1 ( $K_{i,app} = 3900$  nM). Selectivity over MetAP1 is striking because both enzymes share relatively similar active site topography.<sup>13</sup> A structural rationale for this selectivity will be discussed later. Mechanistic enzymology studies determined MetAP2 binding for this 1,2,4-triazole to be competitive.

In analyzing the MetAP2 inhibitory activities from the 12 × 8 array, there are several SAR trends that were evident. First, with respect to substitution on the aniline ring of lead **6**, addition of a methyl group to either the *ortho*- or the *para*-positions of the aniline led to a 10-fold increase in potency, as evidenced by analogs **13** and **23**. Varying the electronic nature of the aniline substituent produced modest effects on potency. Substitution of the *para*-position of the aniline with an electron donating group such as methoxy (**46**) led to a 10-fold enhancement in activity ( $K_{i,app} = 50$  pM) relative to lead **6**. Addition of

Table 1. SAR for 8 × 12 Triazole Array

compd	R1	R2	MetAP2 $K_{i,app}^a$ (nM)	compd	R1	R2	MetAP2 $K_{i,app}^a$ (nM)
6	Ph	Ph	0.5	53	4-OMe-Ph	-CH=C(CH <sub>3</sub> ) <sub>2</sub>	0.16
12	Ph	thiophen-2-yl	0.75	54	4-OMe-Ph	5-methyl-3-isoxazol-3-yl	1.6
13	2-Me-Ph	Ph	0.04	55	3,4-OMe-Ph	Ph	1.7
14	2-Me-Ph	2-Me-Ph	2.5	56	3,4-OMe-Ph	2-Me-Ph	18
15	2-Me-Ph	2-MeO-Ph	61	57	3,4-OMe-Ph	2-MeO-Ph	> 1000
16	2-Me-Ph	2-F-Ph	0.23	58	3,4-OMe-Ph	2-F-Ph	1.3
17	2-Me-Ph	3,4-difluoro-Ph	2.4	59	3,4-OMe-Ph	3,4-difluoro-Ph	4.0
18	2-Me-Ph	4-pyridyl	3.7	60	3,4-OMe-Ph	2-pyridyl	24
19	2-Me-Ph	cyclohexyl	3.3	61	3,4-OMe-Ph	4-pyridyl	9.6
20	2-Me-Ph	-CH=C(CH <sub>3</sub> ) <sub>2</sub>	0.15	62	3,4-OMe-Ph	cyclohexyl	8.3
21	2-Me-Ph	2-methyl-thiazo-4-yl	3.8	63	3,4-OMe-Ph	-CH=C(CH <sub>3</sub> ) <sub>2</sub>	0.9
22	2-Me-Ph	5-methyl-3-isoxazol-3-yl	3.6	64	3,4-OMe-Ph	2-methyl-thiazo-4-yl	21
23	4-Me-Ph	Ph	0.07	65	3,4-OMe-Ph	5-methyl-3-isoxazol-3-yl	7.0
24	4-Me-Ph	2-Me-Ph	6.5	66	4-CO <sub>2</sub> Me-Ph	Ph	0.7
25	4-Me-Ph	2-MeO-Ph	> 10 000	67	4-CO <sub>2</sub> Me-Ph	2-Me-Ph	135
26	4-Me-Ph	2-F-Ph	0.65	68	4-CO <sub>2</sub> Me-Ph	2-MeO-Ph	10
27	4-Me-Ph	3,4-difluoro-Ph	3.3	69	4-CO <sub>2</sub> Me-Ph	2-F-Ph	0.41
28	4-Me-Ph	2-pyridyl	7.8	70	4-CO <sub>2</sub> Me-Ph	3,4-difluoro-Ph	1.3
29	4-Me-Ph	4-pyridyl	5.7	71	4-CO <sub>2</sub> Me-Ph	2-pyridyl	0.9
30	4-Me-Ph	cyclohexyl	100	72	4-CO <sub>2</sub> Me-Ph	4-pyridyl	0.9
31	4-Me-Ph	-CH=C(CH <sub>3</sub> ) <sub>2</sub>	1.2	73	4-CO <sub>2</sub> Me-Ph	cyclohexyl	2.7
32	4-Me-Ph	2-methyl-thiazo-4-yl	7.8	74	4-CO <sub>2</sub> Me-Ph	-CH=C(CH <sub>3</sub> ) <sub>2</sub>	0.5
33	4-Me-Ph	5-methyl-3-isoxazol-3-yl	3.5	75	4-CO <sub>2</sub> Me-Ph	2-methyl-thiazo-4-yl	3.8
34	4-Me-Ph	thiophen-2-yl	5.2	76	4-CO <sub>2</sub> Me-Ph	5-methyl-3-isoxazol-3-yl	0.8
35	4-Cl-Ph	Ph	0.43	77	2-(Ph)-Ph	Ph	740
36	4-Cl-Ph	2-Me-Ph	23	78	2-(Ph)-Ph	2-Me-Ph	> 2000
37	4-Cl-Ph	2-MeO-Ph	> 10 000	79	2-(Ph)-Ph	2-MeO-Ph	> 2000
38	4-Cl-Ph	2-F-Ph	0.61	80	2-(Ph)-Ph	2-F-Ph	350
39	4-Cl-Ph	3,4-difluoro-Ph	1.5	81	2-(Ph)-Ph	3,4-difluoro-Ph	> 2000
40	4-Cl-Ph	2-pyridyl	4.0	82	2-(Ph)-Ph	4-pyridyl	> 2000
41	4-Cl-Ph	4-pyridyl	2.5	83	2-(Ph)-Ph	cyclohexyl	650
42	4-Cl-Ph	cyclohexyl	5.2	84	2-(Ph)-Ph	-CH=C(CH <sub>3</sub> ) <sub>2</sub>	480
43	4-Cl-Ph	-CH=C(CH <sub>3</sub> ) <sub>2</sub>	0.52	85	2-(Ph)-Ph	5-methyl-3-isoxazol-3-yl	1700
44	4-Cl-Ph	2-methyl-thiazo-4-yl	4.8	86	3-pyridyl	Ph	0.04
45	4-Cl-Ph	5-methyl-3-isoxazol-3-yl	1.8	87	3-pyridyl	2-Me-Ph	1.7
46	4-OMe-Ph	Ph	0.05	88	3-pyridyl	2-F-Ph	0.3
47	4-OMe-Ph	2-MeO-Ph	34	89	3-pyridyl	3,4-difluoro-Ph	0.5
48	4-OMe-Ph	2-F-Ph	0.13	90	3-pyridyl	2-pyridyl	5.7
49	4-OMe-Ph	3,4-difluoro-Ph	2.1	91	3-pyridyl	4-pyridyl	3.0
50	4-OMe-Ph	2-pyridyl	18	92	3-pyridyl	cyclohexyl	6.5
51	4-OMe-Ph	4-pyridyl	6.1	93	3-pyridyl	2-methyl-thiazo-4-yl	9.1
52	4-OMe-Ph	cyclohexyl	3.1	94	3-pyridyl	5-methyl-3-isoxazol-3-yl	1.5

<sup>a</sup> The statistical error for  $K_{i,app}$  values was in the range of  $\pm 5$ –10% of the reported value from two independent experiments (separate study dates).

Scheme 3. Synthesis of *N*-methyl-triazoles<sup>a</sup>

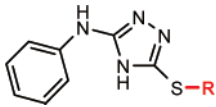
<sup>a</sup> Reagents and conditions: (a) NaH, DMF; MeI, rt, 81%; (b) NaH, DMF; ClCH<sub>2</sub>OEt, rt, 66%; (c) NaH, DMF; MeI, rt, 52%; (d) trifluoroacetic acid, rt, 82%.

a second methoxy group to **46**, exemplified by 3,4-dimethoxyaniline **55**, decreased potency slightly relative to the lead **6**. *para*-Substitution of the aniline ring with electron withdrawing groups such as chloride (**35**) and ester (**66**) afforded activity comparable

to lead **6**. In contrast to the *ortho*-methyl aniline analogs (**13**, **14**, **16**–**22**), the *ortho*-phenyl anilines (**77**–**85**) were found to be much less active by two to three orders of magnitude in relation to lead **6**. Replacement of the aniline phenyl ring in **6** with a 3-pyridyl ring (**86**) resulted in a 10-fold enhancement in potency.

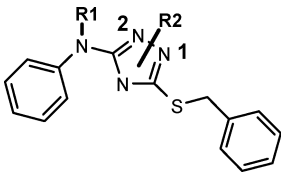
With respect to substitution of the benzyl group of lead **6**, substitution at the *ortho*-position was not well tolerated. A 10-fold decrease in activity was observed for 2-methyl-benzyl analogs (**24**, **36**, and **56**), and at least a 100-fold decrease or more was observed for 2-methoxy-benzyl analogs (**15**, **25**, and **37**). Substitution of the benzyl group of **6** with electron-withdrawing groups such as 2-fluoro or 3,4-difluoro (**16**, **38**, and **89**) did not lead to a significant change in potency ( $\sim 5$ -fold or less) across aniline templates. Replacement of the benzyl group with the smaller but equally rigid and lipophilic isoprenyl group in most cases maintained activity (**20**, **43**, **53**, and **74**) compared to the lead **6**. However, substitution with the more conformationally flexible, lipophilic, cyclohexylmethyl group generally led to a 5–10-fold decrease in activity across each aniline series (**19**, **42**, **73**, and **92**) relative to lead **6**. Replacement

Table 2. 5-Alkylthio Analogs



cmpd	R	MetAP2 $K_{i,app}^a$ (nM)
<b>6</b>	Bn	0.5
<b>99</b>	Me	1000
<b>100</b>	-CH <sub>2</sub> -CH <sub>2</sub> -CH(CH <sub>3</sub> ) <sub>2</sub>	66
<b>101</b>	-CH <sub>2</sub> -CH=CH(CH <sub>3</sub> ) <sub>2</sub>	1

<sup>a</sup> The statistical error for  $K_{i,app}$  values was in the range of  $\pm 5$ –10% of the reported value from two independent experiments (separate study dates).

Table 3. *N*-methylated Analogs


cmpd	R1	R2		MetAP2 $K_{i,app}^a$ (nM)
		N1	N2	
<b>95</b>	H		Me	1300
<b>96</b>	H	Me		> 10 000
<b>98</b>	Me			15

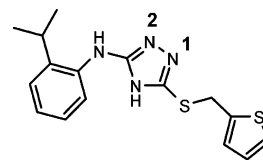
<sup>a</sup> The statistical error for  $K_{i,app}$  values were in the range of  $\pm 5$ –10% of the reported value from two independent experiments (separate study dates).

of the phenyl ring in the sulfur side-chain of **6**, with heterocyclic rings such as isoxazole, pyridine, thiazole, and thiophene, led to decreases in binding affinity of 5–15-fold, depending on the aniline group with which it was combined. This is best exemplified by analogs **18**, **32**, **44**, **51**, **65**, and **93**.

To firmly establish whether or not the benzyl group in **6** is the optimal thio-ether side-chain, a series of simplified *S*-alkylated analogs of **6** were synthesized (Table 2). Replacement of the benzyl group with methyl (**99**) led to a 1000-fold decrease in potency. Installation of a simple aliphatic chain such as 3-methyl-butyl (**100**;  $K_{i,app}$  = 66 nM) regained a portion of the activity back, however, the net result was still a 100-fold loss of activity in relation to lead **6**. Introduction of unsaturation (isoprenyl; **101**) restored activity relative to the lead **6**. These results reveal that a benzylic group or allylic olefins are key functionalities required for tight inhibitor binding.

Substitution on the aniline or triazole nitrogens resulted in a significant decrease in potency (Table 3). This is not surprising given the presumed coordination of one or more of these nitrogens to the active-site cobalt ions. Methylation of the aniline nitrogen, exemplified by **98**, resulted in only a 30-fold decrease in activity relative to the initial screening lead **6**, suggesting that the aniline N–H is not critical for inhibitor binding. However, substitution on N2 (**95**) gave rise to a 1000-fold decrease in potency, while installation of a methyl group at N1 (**96**) of the heterocyclic ring abolished activity completely, thus indicating that these two triazole nitrogen atoms play an important role in binding.

The X-ray crystal structure of inhibitor **102** (Figure 2) bound in the active site of human MetAP2 confirmed the critical role the two contiguous triazole nitrogens play in coordinating to the Co<sup>2+</sup> ions, with close contacts (2.19, 2.16 Å) observed between both cobalt atoms, N1, and N2 of the triazole ring.



**102**;  $K_{i,app}$  = 2 nM

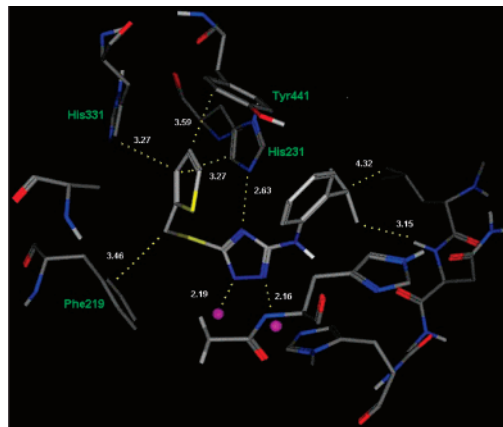
Figure 2. Thiophene **102**.

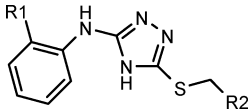
Figure 3. Triazole **102** in the active site of MetAP2; distances between inhibitor and active site residues are shown.

The remaining nitrogen of the triazole ring is in suitable proximity (2.63 Å) to the histidine nitrogen of His-231 for hydrogen bonding. This interaction was found to be critical because mutation of His-231 to Ala in human MetAP2 (data not shown) completely abolished inhibitory activity in this chemical series. The *S*-thienylmethyl side-chain of **102** occupies a hydrophobic pocket defined structurally by Phe-219, His-331, and Tyr-444 as well as His-231. The enhanced potency observed for compounds containing benzylic or allylic substituents on the sulfur atom appears to be the result of favorable  $\pi$ – $\pi$  interactions between the inhibitor and these aromatic/heteroaromatic amino acid residues. The close proximity of His-231 and His-331 to the thiophene ring also confirms why phenyl substituents such as *ortho*-methoxy (compounds **25**, **37**, and **57**) are not well tolerated on the phenyl group of the *S*-benzyl side-chain. The *S*-benzyl binding pocket may indeed be responsible for the specificity observed for triazole inhibition of MetAP2 versus MetAP1, as this pocket is narrower in MetAP1 and may only be able to accept a methionine side-chain as opposed to a larger *S*-benzyl group.<sup>13</sup> The *ortho*-isopropyl-aniline ring, positioned to the right of Tyr-441 and flanked on its left by the protein backbone, is oriented toward the pocket opening and, thus, is largely exposed to solvent. It is not too surprising that a variety of alkyl and polar groups may be accommodated at the *ortho*-, *meta*-, and *para*-positions of the aniline in lead **6**, as evidenced by the excellent potency observed for compounds **13**, **23**, **35**, **46**, **55**, and **66**. However *ortho*-phenyl-aniline analogs of lead **6**, such as **77** and **84**, are much weaker in activity as compared to *ortho*-methyl-anilines **13** and **20**, suggesting that the *ortho*-phenyl substituent may interact unfavorably with the nearby protein. This hypothesis is supported by the close proximity of the isopropyl group of **102** to the backbone (Asn 329, Leu 328) of the protein (Figure 3).

### Cellular and Tissue Activity

Angiogenesis, the process by which blood vessels form, is known to be essential for the growth of solid tumors.<sup>2</sup> Liu's laboratory has shown that the irreversible MetAP2 inhibitor,



**Table 4.** Functional Activity of Triazole Analogs in Endothelial Cells


cmpd	R1	R2	mMetAP2 <sup>a</sup>	hMetAP2 <sup>b</sup>	MS-1	HUVEC
			K <sub>i,app</sub>	K <sub>i,app</sub>	IC <sub>50</sub> <sup>c</sup>	IC <sub>50</sub> <sup>c</sup>
<b>6</b>	H	Ph	2	0.5	3000	3000
<b>103</b>	<i>i</i> -Pr	2-furan	5	3	100	30
<b>104</b>	<i>i</i> -Pr	3-furan	20	24	140	40
<b>2a</b>				1		0.2

<sup>a</sup> m = murine. All data in nM. <sup>b</sup> h = human. All data in nM. <sup>c</sup> The statistical error was in the range of  $\pm 5$ –10% of the reported value from at least three independent growth inhibition experiments.

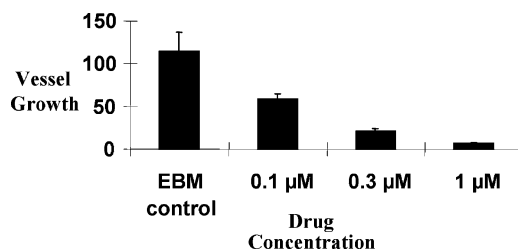
**Table 5.** M<sup>2+</sup>-MetAP2 Enzyme vs HUVEC Activity<sup>a</sup>

cmpd	Co <sup>2+</sup> -hMetAP2 <sup>b</sup>	Mn <sup>2+</sup> -hMetAP2 <sup>b</sup>	HUVEC
	K <sub>i,app</sub>	K <sub>i,app</sub>	IC <sub>50</sub> <sup>c</sup>
<b>6</b>	0.5	180	1000
<b>12</b>	0.8	630	2000
<b>102</b>	2	1500	150
<b>103</b>	3	1500	30
<b>104</b>	24	1800	40

<sup>a</sup> M = metal. <sup>b</sup> hMetAP2 = human MetAP2. All data in nM. <sup>c</sup> The statistical error was in the range of  $\pm 5$ –10% of the reported value from at least three independent growth inhibition experiments.

**2a**, inhibits the growth or proliferation of endothelial cells, the primary cell type involved in vascularization.<sup>2</sup> The lead 1,2,4-triazole compound, **6**, was also found to be an inhibitor of endothelial cell proliferation when studied in an XTT<sup>14</sup> assay, however, it unexpectedly exhibited a three to four order of magnitude shift between human MetAP2 enzyme and endothelial cell (HUVEC) potency. A similar shift in potency was observed between murine MetAP2 enzyme and murine stroma cell (MS-1) activity. Interestingly, furan analogs of **6** (**103** and **104**) were found to be potent inhibitors of human endothelial cell proliferation. Unlike lead **6**, the cellular activity for triazoles **103** and **104** compared favorably (one order of magnitude shift) with both the murine and the human Co<sup>2+</sup>-MetAP2 enzyme inhibitory activity (Table 4). A possible explanation for the close similarity between potencies obtained for enzyme and cell growth inhibition in the furan series may be a favorable change in physicochemical properties, thus enabling these analogs more facile access (cell permeability) to the intracellular site of action.

Recent reports suggest the physiologically relevant human MetAP2 metal to be manganese, which may explain the discrepancy between enzyme and cellular potency observed for our lead **6**.<sup>2e,7c,7e</sup> In light of these reports, we also evaluated a set of compounds against recombinant Mn<sup>2+</sup>-MetAP2 (Table 5). HUVEC cellular potency for analogs **6** and **12** was discovered to be in line with their Mn<sup>2+</sup> enzyme inhibitory potencies (only 5–10-fold attenuated), however, greater than a 100-fold difference exists versus Co<sup>2+</sup> enzyme inhibitory potencies. By itself, this data would seem to indicate that Mn<sup>2+</sup> is the relevant metal. However, the cellular potency for thiophene **102** was found to be similar to enzyme potency for both metalloenzymes (roughly one order of magnitude difference, although closer to the Mn<sup>2+</sup>-MetAP2 inhibitory potency), bringing into question that the Mn<sup>2+</sup>-MetAP2 is the relevant cellular form and suggesting that neither enzyme activity is correlative with cellular activity. Interestingly, HUVEC activity for furan analogs **103** and **104** was found to be more correlative ( $\leq 10$ -fold difference) with the Co<sup>2+</sup>-MetAP2 enzyme activity, and conversely, the corresponding Mn<sup>2+</sup>-MetAP2 enzyme activity was attenuated by 50-fold. It is clear that these results

**Figure 4.** Dose-dependent inhibition of angiogenesis by **104** in an aortic ring assay.

do not shed light on which metallo-enzyme activity more accurately predicts activity in cells. The observation that MetAP2 is catalytically active when complexed to a variety of endogenous metal cofactors,<sup>2e,7c</sup> such as Co<sup>2+</sup>, Fe<sup>2+</sup>, Mn<sup>2+</sup>, Ni<sup>2+</sup>, and Zn<sup>2+</sup>, highlights the difficulty in determining the physiologically relevant metalloprotease. Adding an additional element of complexity, Hanzlik and co-workers<sup>6</sup> have recently shown that monometalated *E. coli* Mn<sup>2+</sup>-MetAP exhibits full catalytic activity, a discovery that raises the possibility that human MetAP2 could also be monometalated. In a cellular environment, predicting which endogenous metal-enzyme species is present may not be that straightforward and could be dependent not only on cell type, but also surrounding tissue and the concentration of different metal ions found within. The implication is that there may be multiple metallo-MetAP2 species that are naturally occurring, and therefore, pinpointing the most relevant one that affects angiogenesis or cell proliferation may be a challenge. However, the lack of a clear correlation within the cellular results does also suggest other possibilities, such as whether or not this particular class of inhibitors is truly exhibiting their antiproliferative effects through MetAP2 (off-target activity)? This is difficult to determine unequivocally given the issues discussed above, but the observation that analogs such as **103** and **104** exhibit good activity across enzyme, cellular, and angiogenesis assays (data disclosed below) is promising and merits continued focus on MetAP2 as the putative target for this class of anilino-triazoles.

To further investigate the potential of these molecules as antiangiogenic agents, triazole **104** was evaluated in an aortic ring tissue model, an angiogenesis model that examines the ability of a compound to inhibit the growth of blood vessels sprouting from aortic tissue localized in culture. Confocal microscopy was used to quantitate the vessel/sprout area; fluorescent labeling of the sprout area is depicted in Figure 5. The triazole **104** demonstrated dose-dependent inhibition of new blood vessel growth, with near complete inhibition of angiogenesis at 1.0 μM (Figure 4). Triazole **103** also exhibited similar dose-dependent activity in the same model (data not shown). These results establish the utility of anilino-1,2,4-triazole MetAP2 inhibitors as potential therapeutic agents for inhibiting the process of angiogenesis.

## Conclusion

Highly potent anilino-1,2,4-triazole MetAP2 inhibitors have been discovered through high-throughput screening. An efficient parallel array synthesis of triazoles led to rapid SAR development. A variety of sulfur substitutions were combined with different anilino-triazole templates to produce analogs with subnanomolar human MetAP2 inhibitory activity. The deleterious effects on inhibitor potency by methylation of the anilino-triazole nitrogens, as well as the X-ray crystal structure of triazole **102** bound in the active site of MetAP2, confirm the key interactions between the triazole nitrogens, the active site

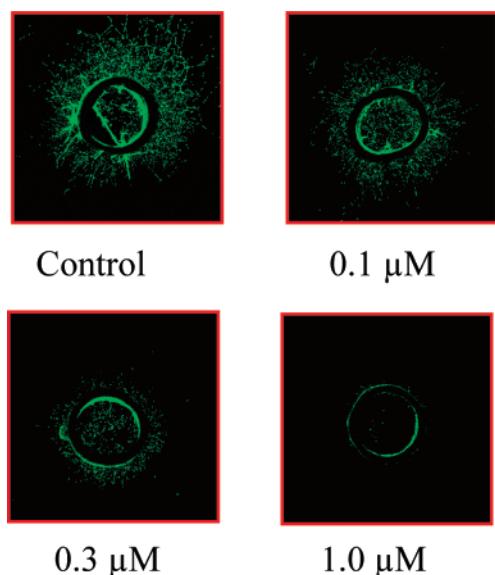


**Figure 5.** Inhibition of angiogenesis by **104** in the rat aortic ring model. Fluorescent (calcein) labeling of aortic ring sprouts under confocal microscopy is shown (0.1–1.0  $\mu\text{M}$  concentrations).

cobalt ions, and His-231. The X-ray structure has also provided a rationale for interpreting SAR within the triazole series. Well-defined side-chain pockets that flank the cobalt ions in the MetAP2 active site prevent extensive *ortho*-substitution of the aromatic rings on the *S*-benzyl and aniline groups contained within lead **6**. Based on the crystal structure, enhanced potency for analogs containing benzylic or allylic substituents on the sulfur atom appears to be the result of favorable  $\pi$ - $\pi$  interactions between the inhibitor and the aromatic/heteroaromatic amino acid residues, which define a hydrophobic pocket in the MetAP2 active site. Triazole analogs **103** and **104**, which possess furanymethyl side-chains, were discovered to be potent inhibitors of human endothelial cell proliferation. Analogs **103** and **104** were also found to dose-dependently inhibit new blood vessel growth in an aortic tissue model of angiogenesis. Although a tight correlation between enzyme (single metallo-MetAP2 species) and cellular activity could not be established, the successful identification of new human MetAP2 inhibitors that inhibit cell proliferation and angiogenesis does underscore the value in considering multiple metalloenzyme species when MetAP2 screening. This work demonstrates the utility of triazoles as potent inhibitors of methionine aminopeptidase-2 and, in addition, validates the strategy of employing heterocycles as key pharmacophores for drug design around metalloenzymes.

## Experimental Section

**Chemistry.** All reagents and solvents were purchased from Aldrich Chemical Co. (or other commercial sources) and used as received. Kieselgel 60 silica gel was used for chromatography. Preparative HPLC purification was performed with a YMC CombiPrep ODS-A column using a gradient of  $\text{CH}_3\text{CN}/\text{H}_2\text{O}$  as eluant and UV detection at 214 nm. Analytical (Anal.) HPLC was performed using two diverse HPLC systems: Method 1) 15–45%  $\text{CH}_3\text{CN}/\text{H}_2\text{O}$  gradient over 6 min (8 min total run) using a  $3.0 \times 50$  mm XTERRA RP C18 column, and Method 2) 40–70%  $\text{MeOH}/0.1 \text{ NH}_4\text{OAc}$  in  $\text{H}_2\text{O}$  gradient over 6 min (8 min total run) using a  $3.0 \times 50$  mm GEMINI C18 column. LCMS mass spectra were taken on a PE Sciex API-150 instrument using electrospray ionization (ESI). Elemental analysis was performed by Quantitative Technologies, Inc.  $^1\text{H}$  NMR and  $^{13}\text{C}$  NMR were recorded at 400 and 100 MHz, respectively, on a Bruker NMR spectrometer. Positive ion mass spectra (HRMS) were acquired as accurate mass

centroid data using a Micromass Q-ToF 2 hybrid quadrupole time-of-flight mass spectrometer equipped with a Z-spray interface over a mass range of 80–1200 Da, with a scan time of 0.95 s and an interscan delay of 0.07 s (ionization was achieved with a spray voltage of 3 kV, a cone voltage of 30 V, with cone and desolvation gas flows of 5–10 and 500 L/hour, respectively).

**General Procedure. Preparation of 3-Anilino-5-benzylthio-1,2,4-triazole (6).** (A) **1-Phenyl-2,4-dithiobiuret (7)**. To a stirring solution of NaOH (0.52 g, 13.1 mmol) in 60 mL of 10%  $\text{H}_2\text{O}$  in  $\text{CH}_3\text{CN}$  was added thiourea (1.0 g, 13.1 mmol). The resulting suspension was heated to 40  $^\circ\text{C}$  for 20 min and then cooled to room temperature. To this mixture was added phenylisothiocyanate (1.5 mL, 13.1 mmol), and the clear yellow solution was stirred overnight. After stirring for 12 h, 1 N HCl was added until a white precipitate formed. The precipitate was filtered, washed with  $\text{H}_2\text{O}$ , and dried under vacuum to produce the title compound as a light yellow powder (0.78 g, 30%).  $^1\text{H}$  NMR (400 MHz,  $\text{DMSO}-d_6$ )  $\delta$  7.25 (t, 2H,  $J = 7.3$  Hz), 7.40 (t, 2H,  $J = 7.9$  Hz), 7.56 (d, 1H,  $J = 7.9$  Hz), 9.13–9.29 (br s, 1H), 10.26–10.79 (br s, 2H).

(B) **2-Ethyl-1-phenyl-2-isodithiobiuret (9)**. To a stirring solution of compound **7** from step A (150 mg, 0.70 mmol) in 4 mL of DMF was added triethylamine (57  $\mu\text{L}$ , 0.70 mmol). The resulting yellow/green solution was stirred for 10 min at room temperature. To this solution was added ethyl iodide (100  $\mu\text{L}$ , 0.70 mmol), and the reaction mixture was stirred for 2 h at room temperature. The yellow solution was poured into 20 mL of  $\text{H}_2\text{O}$  and extracted four times with EtOAc. The organic extracts were dried over  $\text{Na}_2\text{SO}_4$ , filtered, and concentrated, and the crude residue was subjected to column chromatography (silica gel; ethyl acetate/hexane) to afford the title compound as a white solid (108 mg, 64%).  $^1\text{H}$  NMR (400 MHz,  $\text{DMSO}-d_6$ )  $\delta$  1.22 (t, 3H,  $J = 7.2$  Hz), 2.96 (q, 2H,  $J = 7.2$  Hz), 6.85 (d, 1H,  $J = 7.6$  Hz), 7.16 (t, 1H,  $J = 7.2$  Hz), 7.29–7.41 (m, 3H), 8.27 (br s, 1H), 9.89 (br s, 1H), and 10.99 (br s, 1H).

(C) **3-Anilino-5-mercapto-1,2,4-triazole (11)**. To a stirring solution of 2-ethyl-1-phenyl-2-isodithiobiuret **9** (250 mg; 1.03 mmol) in 2.5 mL of EtOH and 0.25 mL of AcOH was added 150  $\mu\text{L}$  of anhydrous hydrazine. The reaction mixture was heated at 80  $^\circ\text{C}$  for 1 h and then cooled to room temperature. To the reaction mixture was added 5 mL of  $\text{H}_2\text{O}$ , and excess concd HCl was added dropwise until a precipitate formed. The precipitate was collected and subsequently dried (under vacuum) to afford the title compound as a white solid (90 mg, 45%). MS (ESI) 190.90 ( $\text{M} - \text{H}$ ) $^+$ .

(D) **3-Anilino-5-benzylthio-1,2,4-triazole (6)**. To a stirring solution of compound **11** from step C (23 mg, 0.12 mmol) in 1.2 mL of DMF was added  $\text{K}_2\text{CO}_3$  (17 mg, 0.12 mmol), followed by benzyl bromide (20 mg, 0.12 mmol). The mixture was stirred overnight, filtered, and purified by preparative HPLC to afford the title compound as a white solid (30 mg, 70%).  $^1\text{H}$  NMR (400 MHz,  $\text{DMSO}-d_6$ )  $\delta$  9.30 (br s, 1H), 7.47 (d, 2H,  $J = 8.1$  Hz), 7.39 (d, 2H,  $J = 7.3$  Hz), 7.31 (t, 2H,  $J = 7.3$  Hz), 7.23 (q, 3H,  $J = 7.3$  Hz), 6.82 (t, 1H,  $J = 7.3$  Hz), and 4.3 (s, 2H). Anal. ( $\text{C}_{15}\text{H}_{14}\text{N}_4\text{S}$ ) C, H, N.

**3-Anilino-5-benzylthio-2-methyl-1,2,4-triazole (95) and 3-Anilino-5-benzylthio-1-methyl-1,2,4-triazole (96)**. To a stirring solution of 3-anilino-5-benzylthio-1,2,4-triazole **6** (0.20 g, 0.71 mmol) in DMF (4 mL) was added NaH (37 mg, 0.92 mmol). To this mixture was added iodomethane (49  $\mu\text{L}$ , 0.78 mmol), and the solution was stirred overnight. The reaction mixture was poured into  $\text{H}_2\text{O}$  (25 mL) and extracted three times with EtOAc. The EtOAc extracts were dried over  $\text{Na}_2\text{SO}_4$ , filtered, and concentrated. The crude mixture was subjected to column chromatography (silica gel, EtOAc/hexane) to provide the title compounds. Compound **95** was isolated as a clear oil (93 mg, 44%).  $^1\text{H}$  NMR (400 MHz,  $\text{DMSO}-d_6$ )  $\delta$  9.20 (br s, 1H), 7.63 (d, 2H,  $J = 7.6$  Hz), 7.42–6.93 (m, 8H), 5.44 (s, 2H), 4.30 (s, 2H), 3.51 (q, 2H,  $J = 7.1$  Hz), 1.07 (t, 3H,  $J = 7.0$ ). LCMS (ESI) 341 ( $\text{M} + \text{H}$ ) $^+$ . Anal. ( $\text{C}_{16}\text{H}_{16}\text{N}_4\text{S}$ ) C, H, N. Compound **96** was isolated as a light oil (77 mg, 37%).  $^1\text{H}$  NMR (400 MHz,  $\text{DMSO}-d_6$ )  $\delta$  9.33 (br s, 1H), 7.51 (d, 2H,  $J = 8.3$  Hz), 7.42–7.22 (m, 8H), 5.23 (s, 2H), 4.47 (s, 2H), 3.43 (q, 2H,  $J = 7.2$  Hz), 1.04 (t, 3H,  $J = 7.0$  Hz). Anal. ( $\text{C}_{16}\text{H}_{16}\text{N}_4\text{S} \cdot 0.2\text{H}_2\text{O}$ ) C, H, N.

**3-(*N*-Methyl-anilino)-5-benzylthio-1,2,4-triazole (98).** (A) **3-Anilino-5-benzylthio-1-(methyl-ethyl-ether)-1,2,4-triazole and 3-Anilino-5-benzylthio-2-(methyl-ethyl-ether)-1,2,4-triazole (97).** To a stirring solution of 3-anilino-5-benzylthio-1,2,4-triazole **6** (0.68 g, 2.41 mmol) in DMF (8 mL) was added NaH (0.12 g, 3.1 mmol). To this mixture was added chloromethyl ethyl ether (0.25 g, 2.65 mmol), and the mixture was stirred overnight. The reaction mixture was poured into H<sub>2</sub>O (50 mL) and extracted three times with EtOAc. The EtOAc extracts were dried over Na<sub>2</sub>SO<sub>4</sub>, filtered, and concentrated. The crude mixture was subjected to column chromatography (silica gel, EtOAc/hexane) to provide the title compounds as a mixture (**97**) of regioisomers as a light yellow oil (0.58 g, 71%). Isomer 1: <sup>1</sup>H NMR (400 MHz, DMSO-*d*<sub>6</sub>) δ 9.33 (br s, 1H), 7.51 (d, 2H, *J* = 8.3 Hz), 7.42–7.22 (m, 8H), 5.23 (s, 2H), 4.47 (s, 2H), 3.43 (q, 2H, *J* = 7.2 Hz), 1.04 (t, 3H, *J* = 7.0 Hz). LCMS (ESI) 341 (M + H)<sup>+</sup>. Isomer 2: <sup>1</sup>H NMR (400 MHz, DMSO-*d*<sub>6</sub>) δ 9.20 (br s, 1H), 7.63 (d, 2H, *J* = 7.6 Hz), 7.42–6.93 (m, 8H), 5.44 (s, 2H), 4.30 (s, 2H), 3.51 (q, 2H, *J* = 7.1 Hz), 1.07 (t, 3H, *J* = 7.0). LCMS (ESI) 341 (M + H)<sup>+</sup>.

**(B) 3-(*N*-Methyl-anilino)-5-benzylthio-1,2,4-triazole (98).** To a stirring solution consisting of a mixture of 3-anilino-5-benzylthio-1-(methyl-ethyl-ether)-1,2,4-triazole and 3-anilino-5-benzylthio-2-(methyl-ethyl-ether)-1,2,4-triazole (**97**; 50 mg, 0.15 mmol) in THF (1 mL) was added NaH (11.8 mg, 0.30 mmol), and to this solution was added iodomethane (0.036 mL, 0.57 mmol). The reaction mixture was stirred overnight. THF was removed (via rotary evaporation under vacuum) and trifluoroacetic acid (0.5 mL) was added to the crude product. The mixture was stirred overnight. Trifluoroacetic acid was removed under vacuum, and the mixture was purified by preparative HPLC to afford the title compound as a clear oil (28 mg, 53%). <sup>1</sup>H NMR (400 MHz, DMSO-*d*<sub>6</sub>) δ 3.3–7.25 (m, 10H), 4.27 (s, 2H), 3.40 (s, 3H). LCMS (ESI) 297 (M + H)<sup>+</sup>. HRMS calcd for C<sub>16</sub>H<sub>16</sub>N<sub>4</sub>S [M]<sup>+</sup>, 296.1095; found, 296.1094. Anal. HPLC: method 1, 99.2%; method 2, 99.2%.

**3-Anilino-5-methylthio-1,2,4-triazole (99).** Compound **99** was prepared according to the General Procedure except methyl iodide was used in step D instead of benzyl bromide. LCMS (ESI) (M + H)<sup>+</sup>. Anal. (C<sub>9</sub>H<sub>10</sub>N<sub>4</sub>S) C, H, N.

**3-Anilino-5-(3-methyl-butylthio)-methylthio-1,2,4-triazole (100).** Compound **100** was prepared according to the General Procedure except 1-bromo-3-methylbutane was used in step D instead of benzyl bromide. LCMS (ESI) (M + H)<sup>+</sup>. Anal. (C<sub>13</sub>H<sub>18</sub>N<sub>4</sub>S) C, H, N.

**3-(Anilino)-5-(3-methyl-2-butenylthio)-1,2,4-triazole (101).** Compound **101** was prepared according to the General Procedure except 1-bromo-3-methyl-2-butene was used in step D instead of benzyl bromide. LCMS (ESI) (M + H)<sup>+</sup>. Anal. [(C<sub>13</sub>H<sub>16</sub>N<sub>4</sub>S)·0.1H<sub>2</sub>O] C, H, N.

**3-[2-(Isopropyl)-anilino]-5-(thiophen-2-ylmethylthio)-1,2,4-triazole (102).** Compound **102** was prepared according to the General Procedure except 2-isopropylphenyl-isothiocyanate was used in step A instead of phenylisothiocyanate, and 2-(chloromethyl)-thiophene was used in step D instead of benzyl bromide. LCMS (ESI) (M + H)<sup>+</sup>. Anal. (C<sub>16</sub>H<sub>18</sub>N<sub>4</sub>S<sub>2</sub>) C, H, N.

**3-[2-(Isopropyl)-anilino]-5-(furan-2-ylmethylthio)-1,2,4-triazole (103).** Compound **103** was prepared according to the General Procedure except 2-isopropylphenyl-isothiocyanate was used in step A instead of phenylisothiocyanate, and 2-(chloromethyl)-furan was used in step D instead of benzyl bromide. LCMS (ESI) (M + H)<sup>+</sup>. HRMS calcd for C<sub>16</sub>H<sub>18</sub>N<sub>4</sub>OS [M]<sup>+</sup>, 315.1280; found, 315.1279. Anal. HPLC: method 1, 99.4%; method 2, 99.3%.

**3-[2-(Isopropyl)-anilino]-5-(furan-3-ylmethylthio)-1,2,4-triazole (104).** Compound **104** was prepared according to the General Procedure except 2-isopropylphenyl-isothiocyanate was used in step A instead of phenylisothiocyanate, and 3-(chloromethyl)-furan was used in step D instead of benzyl bromide. LCMS (ESI) (M + H)<sup>+</sup>. Anal. [(C<sub>16</sub>H<sub>18</sub>N<sub>4</sub>OS)·0.1H<sub>2</sub>O] C, H, N.

**Enzyme Inhibition Assay.** Human methionine aminopeptidase 1 and 2, as well as murine methionine aminopeptidase 2 were isolated as described previously<sup>2e,7f</sup> in the presence of Co<sup>2+</sup>. MetAP2 activity was monitored by measuring the initial velocity of turnover

of the artificial substrate L-methionine-7-amido-4-methylcoumarin (Met-AMC)<sup>2e</sup>. Assays were performed in 96-well microtiter plates using recombinant N-terminal truncated human methionine aminopeptidase 2, with Co<sup>2+</sup> as a cofactor. In a typical 96-well plate assay, the increase in the fluorescence emission ( $\lambda_{\text{ex}} = 360$  nm,  $\lambda_{\text{em}} = 460$  nm) of a 50  $\mu$ L assay solution in each well was monitored continuously using a Cytofluor series 4000 multiwell plate reader (PerSeptive Biosystems) and used to calculate the initial velocity of hMetAP2. Each 50  $\mu$ L assay solution contained 50 mM HEPES·Na<sup>+</sup> (pH 7.5), 100 mM NaCl, 10 nM purified MetAP2 enzyme, and 0.4 mM Met-AMC (in 1% DMSO aqueous solution,  $K_m = 0.3$  mM with Co<sup>2+</sup> as a cofactor). Assays were initiated with the addition of substrate, and the initial rates were corrected for the background rate determined in the absence of MetAP2.  $K_{i,\text{app}}$  data was fitted to the Dixon competitive inhibition equation (eq 1) using Grafit (Erithacus software), in which  $v_0$  represents the initial velocity of the reaction,  $K_m$  represents the Michaelis–Menton constant of MetAP2,  $V_{\text{max}}$  represents the maximum turnover rate of MetAP2,  $I$  represents the concentration of inhibitors, and  $S$  represents the substrate of MetAP2.

$$1/v_0 = K_m \times I / (V_{\text{max}} \times S \times K_{i,\text{app}}) + (1/V_{\text{max}}) \times (1 + K_m/S) \quad (1)$$

For use in the manganese activation assay, the cobalt metal was removed from human MetAP2 by treatment with EDTA.<sup>15</sup> MetAP2 activity was monitored by measuring the initial velocity of turnover of the artificial substrate L-methionine-7-amido-4-trifluoromethylcoumarin (Met-AFC). Assays were performed in 96-well microtiter plates using recombinant N-terminal truncated methionine aminopeptidase 2 with 25  $\mu$ M Mn<sup>2+</sup> added as cofactor. In a typical 96-well plate assay, the increase in the fluorescence emission ( $\lambda_{\text{ex}} = 405$  nm,  $\lambda_{\text{em}} = 530$  nm) of a 50  $\mu$ L assay solution in each well was monitored and used to calculate the initial velocity of MetAP2. Each 50  $\mu$ L assay solution contained 50 mM HEPES·Na<sup>+</sup> (pH 7.5), 100 mM NaCl, 23 nM purified MetAP2 enzyme, and 2 mM Met-AFC (in 1% DMSO aqueous solution,  $K_m = 5$  mM with Mn<sup>2+</sup> as a cofactor). Statistical error for  $K_{i,\text{app}}$  values were in the range of  $\pm 5$ –10% of the reported value from two independent experiments (separate study dates).

**Kinetic Analysis.** Data was fitted to the appropriate rate equations using Grafit computer software. Initial velocity data conforming to Michaelis–Menton kinetics was fitted to eq 2. Inhibition patterns conforming to apparent *competitive and non-competitive inhibition* were fitted to eq 3 and eq 4, respectively.

$$v = VA / (K_a + A) \quad (2)$$

$$v = VA / [K_a(1 + I/K_{is}) + A] \quad (3)$$

$$v = VA / [K_a(1 + I/K_{is}) + A(1 + I/K_{ii})] \quad (4)$$

In eqs 3 and 4,  $v$  is the initial velocity,  $V$  is the maximum velocity,  $K_a$  is the apparent Michaelis constant,  $I$  is the inhibitor concentration, and  $A$  is the concentration of variable substrates. The nomenclature used in the rate equations for inhibition constants is that of Cleland,<sup>17</sup> in which  $K_{is}$  and  $K_{ii}$  represent the apparent slope and intercept inhibition constants, respectively.

**HUVEC and MS-1 Cell Growth Inhibition Assay.** The ability of MetAP2 inhibitors to inhibit cell growth was assessed by the standard XTT microtiter assay. XTT, a dye sensitive to the pH change of mitochondria in eukaryotic cells, is used to quantify the viability of cells in the presence of chemical compounds. Cells seeded at a given number undergo approximately two divisions on average in the 72 h of incubation. In the absence of any compound, this population of cells is in exponential growth at the end of the incubation period; the mitochondrial activity of these cells is reflected in the spectrophotometric readout (A450). Viability of a similar cell population in the presence of a given concentration of compound is assessed by comparing the A450 reading from the test well with that of the control well. Flat-bottomed 96-well plates are seeded with appropriate numbers of cells ( $4$ – $6 \times 10^3$  cells/



well in a volume of 200  $\mu\text{L}$ ) from trypsinized exponentially growing cultures. The wells are coated with matrigel prior to establishing the cultures. To "blank" wells is added growth medium only. Cells are incubated overnight to permit attachment. On the next day, medium from wells that contain cells is replaced with 180  $\mu\text{L}$  of fresh medium. Appropriate dilutions of test compounds are added to the wells, with the final DMSO concentration in all wells being 0.2%. Cells plus compound are incubated for an additional 72 h at 37 °C under the normal growth conditions of the cell line used. Cells are then assayed for viability using standard XTT/PMS prepared immediately before use: 8 mg XTT (Sigma X-4251) per plate is dissolved in 100  $\mu\text{L}$  DMSO.  $\text{H}_2\text{O}$  (3.9 mL) is added to dissolve XTT and 20  $\mu\text{L}$  of PMS stock solution (30 mg/mL) is added from frozen aliquoted stock solution (10 mg of PMS (phenazine methosulfate, Sigma P-9625) in 3.3 mL of PBS without cations; these stocks are frozen at -20 °C until use). XTT/PMS solution (50  $\mu\text{L}$ ) is added to each well and the plates are incubated for 90 min (time required may vary according to cell line, etc.) at 37 °C until  $A_{450}$  is  $> 1.0$ . Absorbance at 450 nm is determined using a 96-well UV plate reader. Percent viability of cells in each well is calculated from these data (having been corrected for background absorbance).  $\text{IC}_{50}$  is that concentration of compound that reduces cell viability to 50% control (untreated) viability. Statistical error for  $\text{IC}_{50}$  values was in the range of  $\pm 5$ –10% of the reported value from at least three independent growth inhibition experiments.

**Aortic Ring Assay. Animals:** 7- to 10-week-old Male Sprague Dawley rats at 7 to 10 weeks of age were purchased from Nippon SLC. **Reagents:** Matrigel, Becton Dickinson Labware; Calcein-AM, Dojindo Laboratory; endothelial cell basal medium (EBM), Clonetics; antibiotic antimycotic solution (100 $\times$ ) stabilized, Sigma. **Equipment:** Culture slide, Becton Dickinson Labware; surgical microscope, Nikon; laser scanning microscope, Carl Zeiss.

Rings of rat thoracic aorta were embedded within Matrigel overlaid with serum-free medium in the presence/absence of inhibitors and were subsequently cultured for 6 days. Cells within capillary-like sprouts were vitally labeled with Calcein-AM/visualized under confocal microscope, thereby enabling quantification of levels of angiogenesis by image analysis.

**Preparation of Rat Aortic Ring Cultures:** Rings of the rat thoracic aortas were prepared as described previously.<sup>16</sup> Thoracic aortas from male Sprague-Dawley (SD) rats at 7–10 weeks of age were dipped in phosphate-buffered saline (PBS) in a culture dish. The periaortic fibroadipose tissue was removed under a dissecting microscope, while care was given not to damage the blood vessel wall. After rinsing with PBS to remove intramural blood clot, rings were made by slicing the aorta with a fine blade by approximately 1 mm long, and the rings were subsequently rinsed three times with serum-free EBM medium. Eight-well chamber slides were kept on ice and coated with 110  $\mu\text{L}$ /well of Matrigel at 4 °C. Matrigel was allowed to gel by incubation at 37 °C for 30 min. Each aortic ring was placed on top of the gel and embedded with an extra 40  $\mu\text{L}$  of ice-cold Matrigel. After incubation at 37 °C for 30 min, each well was overlaid with 500  $\mu\text{L}$  of serum-free medium (EBM) supplemented penicillin (100  $\mu\text{g}/\text{mL}$ ), streptomycin (100  $\mu\text{g}/\text{mL}$ ), and amphotericin B (0.25  $\mu\text{g}/\text{mL}$ ). The rings were cultured for 6 days in an incubator (5%  $\text{CO}_2$ ) at 37 °C with medium change every 3 days.

**Calcein Staining and Image Analysis:** An aliquot of 1  $\mu\text{L}$  of 5 mg/mL calcein in DMSO was mixed with 1 mL of serum-free EBM medium. After brief removal of culture medium from a well of culture slide, 200  $\mu\text{L}$  of calcein/EBM solution was gently added to a well of culture slide. After incubation at 37 °C for 1 h, fluorescent-labeled sprouts were visualized under confocal microscopy. A projected image of aortic-ring sprouts was made from images of ten optical slices (70  $\mu\text{m}$ /each) for each ring. Levels of angiogenesis were represented by fluorescent areas (pixels) beyond the outer rim of each aortic ring.

Calcein-stained image was loaded in the Image-Pro Plus program, an imaging software. The area outside the outer rim of each aortic ring was defined using the Area Of Interest (AOI) tool. The

thresholds range was changed from 40 to 255 to segment the image into objects and background. The sum of measurements for area of the objects was calculated and saved to an Excel file for statistic analysis.

**Immunohistochemistry:** The aortic ring with Matrigel was fixed in 4% paraformaldehyde/PBS overnight at 4 °C. After incubation in 30% sucrose/PBS overnight, the ring was embedded in O.C.T. compound. The sample was frozen on dry ice and cryo-sectioned. For immunohistochemistry, sections were washed three times with 0.3% Triton-X100/PBS and blocked with 3% normal serum /PBS. Sections were incubated with primary antibody at 4 °C overnight. After washing, sections were incubated with Alexa 546-conjugated secondary antibody at 4 °C and washed with 0.3% Triton-X100/PBS. The fluorescence image was detected under confocal microscope.

**Crystallography.** The entire native sequence of the human MetAP2 protein was employed and was purified as described by Liu et al.<sup>13a</sup> Complexes were prepared by introducing solid inhibitor into the crystal mother liquor after crystal formation and then allowed to incubate at 4 °C for 24 to 48 h.

Crystals of human methionineaminopeptidase-2 complexed with inhibitor grew to a size of approximately 0.1–0.2  $\text{mm}^3$  in about 6 days at 4 °C. The concentration of inhibited human methionineaminopeptidase-2 used in the crystallization was approximately 10–15 mg/mL. The method of vapor diffusion in sitting drops was used to grow crystals from the solution of human methionineaminopeptidase-2. Crystals grew at 4 °C from drops containing protein in a solution of 10% glycerol in 10 mM Hepes buffer at pH 7.4 containing 0.15 M NaCl. This solution was mixed in equal volumes with a reservoir solution of 15–20% *tert*-butyl alcohol containing 0.4–0.1 M aqueous sodium citrate at pH 5.5. Crystals of the complex are orthorhombic, space group  $C222_1$ , with cell constants of  $a = 89.7$ ,  $b = 99.7$ , and  $c = 100.6$  Å. The crystals contain one molecule in the asymmetric unit and approximately 54% solvent, with a  $V_m$  value of 2.75  $\text{Å}^3/\text{Dalton}$ . X-ray diffraction data were measured from a single crystal for each inhibitor complex using synchrotron radiation provided by beamline 17-ID at the Advance Photon Source, Argonne National Laboratory. The protein structure for the complex was determined by molecular replacement using CNX (Molecular Simulations, Inc.). The starting model consisted of all protein atoms of the published structure of human methionineaminopeptidase-2 published by Liu et al.<sup>13a</sup> This model was refined by rigid-body refinement, and the resulting phases were used to calculate Fourier maps with coefficients  $|F_o - F_c|$  and  $|2F_o - F_c|$  into which the atomic model of human methionineaminopeptidase-2 was built using the molecular graphics system XtalView (Molecular Simulations, Inc.). Conventional positional refinement was carried out during protein model building using CNX. The density corresponding to the inhibitor was fit to difference Fourier electron density maps with XtalView, and the resulting inhibitor complex structure refined using CNX to a final  $R_c$  value of 0.22 for the inhibitor complex.

**Acknowledgment.** We thank Dr. Yie-Hwa Chang and St. Louis University as the source of the intellectual property for the type 2 human methionine aminopeptidase and Prof. Jon Clardy and Dr. Cristina Nonato for guidance in crystallizing human MetAP2.

**Supporting Information Available:** Crystal structure determination/refinement statistics for **102**, data for key SAR compounds **12–94**, and tabulated elemental analyses/HRMS/HPLC data for all SAR compounds are given. This material is available free of charge via the Internet at <http://pubs.acs.org>.

## References

- (1) (a) Gimbrone, M. A. J.; Leapman, S. B.; Cotran, R. S.; Folkman, J. Tumor dormancy in vivo by neovascularization. *J. Exp. Med.* **1972**, *136*, 261–276. (b) Folkman, J. Tumor Angiogenesis. *Adv. Cancer Res.* **1985**, *43*, 175–203. (c) Folkman, J. Angiogenesis in cancer,



- vascular, rheumatoid and other disease. *Nat. Med.* **1995**, *1*, 27–31.
- (d) Hanahan, D.; Folkman, J. Patterns and emerging mechanisms of the angiogenic switch during tumorigenesis. *Cell* **1996**, *86*, 353–364.
- (e) Risau, W. Mechanisms of angiogenesis. *Nature* **1997**, *386*, 671–674.
- (2) (a) Wingfield, P.; Graber, P.; Turcatti, G.; Movva, N. R.; Pelletier, M.; Craig, S.; Rose, K.; Miller, C. G. Purification and characterization of a methionine-specific aminopeptidase from *Salmonella typhimurium*. *Eur. J. Biochem.* **1989**, *180*, 23–32. (b) Bazan, J. F.; Weaver, L. H.; Roderick, S. L.; Huber, R.; Matthews, B. W. Sequence and structure comparison suggest that methionine aminopeptidase, prolidase, aminopeptidase, and creatinase share a common fold. *Proc. Natl. Acad. Sci. U.S.A.* **1994**, *91*, 2473–2477. (c) Kobayashi, M.; Shimizu, S. Cobalt proteins. *Eur. J. Biochem.* **1999**, *261*, 1–9. (d) Lowther, W. T.; Matthews, B. W. Structure and function of the methionine aminopeptidase. *Biochim. Biophys. Acta* **2000**, *1477*, 157–167. (e) Yang, G.; Kirkpatrick, R. B.; Ho, T.; Zhang, G.; Liang, P.; Johanson, K. O.; Casper, D. J.; Doyle, M. L.; Marino, J. P., Jr.; Thompson, S. K.; Wenfang, C.; Tew, D. G.; Meek, T. D. Steady-state kinetic characterization of substrates and metal-ion specificities of the full-length and N-terminally truncated recombinant human methionine aminopeptidases (type 2). *Biochemistry* **2001**, *40*, 10645–10654.
- (3) (a) Griffith, E. C.; Su, Z.; Turk, B. E.; Chen, S.; Chang, Y. H.; Wu, Z.; Biemann, K.; Liu, J. O. Methionine aminopeptidase (type 2) is the common target for angiogenesis inhibitors AGM-1470 and ovalicin. *Chem. Biol.* **1997**, *4* (6), 461–471. (b) Sin, N.; Meng, L.; Wang, M. Q.; Wen, J. J.; Bornmann, W. G.; Crews, C. M. The anti-angiogenic agent fumagillin covalently binds and inhibits the methionine aminopeptidase, MetAP-2. *Proc. Natl. Acad. Sci. U.S.A.* **1997**, *1094* (12), 6099–6103. (c) Griffith, E. C.; Shuang, S.; Niwayama, S.; Ramsay, C. A.; Chang, Y.; Liu, J. O. Molecular recognition of angiogenesis inhibitors fumagillin and ovalicin by methionine aminopeptidase 2. *Proc. Natl. Acad. Sci. U.S.A.* **1998**, *95*, 15183–15188. (d) Turk, B. E.; Griffith, E. C.; Wolf, S.; Biemann, K.; Chang, Y.; Liu, J. O. Selective inhibition of amino-terminal methionine processing by TNP-470 and ovalicin in endothelial cells. *Chem. Biol.* **1999**, *6* (11), 823–833. (e) Bernier, S. G.; Taghizadeh, N.; Thompson, C. D.; Westlin, W. F.; Hannig, G. Methionine aminopeptidase type I and type II are essential to control cell proliferation. *J. Cell. Biochem.* **2005**, *95* (6), 1191–1203.
- (4) (a) Chang, S. Y.; McGary, E. C.; Chang, S. Methionine aminopeptidase gene *Escherichia* is essential for cell growth. *J. Bacteriol.* **1989**, *171*, 4071–4072. (b) Folkman, J. Clinical applications of research on angiogenesis. *New Engl. J. Med.* **1995**, *333*, 1757–1763. (c) Li, X.; Chang, Y. H. Amino-terminal protein processing in *Saccharomyces cerevisiae* is an essential function that requires two distinct methionine aminopeptidases. *Proc. Natl. Acad. Sci. U.S.A.* **1995**, *92*, 12357–12361. (d) Hannig, G.; Lazarus, D. D.; Bernier, S. G.; Karp, R. M.; Lorusso, J.; Qiu, D.; Labenski, M. T.; Wakefield, J. D.; Thompson, C. D.; Westlin, W. F. Inhibition of melanoma tumor growth by a pharmacological inhibitor of MetAP-2, PPI-2458. *Int. J. of Oncology* **2006**, *28* (4), 955–963.
- (5) (a) Keding, S. J.; Dales, N. A.; Lim, S.; Beaulieu, D.; Rich, D. H. Synthesis of (3R)-amino-(2S)-hydroxy amino acids for inhibition of methionine aminopeptidase-I. *Synth. Commun.* **1998**, *28* (23), 4463–4470. (b) Sheppard, G. S.; Wang, J.; Kawai, M.; BaMaung, N.; Craig, R. A.; Erickson, S. A.; Lynch, L.; Patel, J.; Yang, F.; Searle, X. B.; Lou, P.; Park, C.; Kim, K. H.; Henkin, J.; Lesniewski, R. 3-Amino-2-hydroxyamides and related compounds as inhibitors of methionine aminopeptidase-2. *Bioorg. Med. Chem. Lett.* **2004**, *14* (4), 865–868. (c) Kawai, M.; BaMaung, S. D.; Fidanze, S. A.; Erickson, S. A.; Tedrow, J. S.; Sanders, W. J.; Vasudevan, A.; Park, C.; Hutchins, C.; Comess, K. M.; Kalvin, D.; Wang, J.; Zhang, Q.; Lou, P.; Tucker-Garcia, L.; Bouska, J.; Bell, R. L.; Lesniewski, R.; Henkin, J.; Sheppard, G. S. Development of sulfonamide compounds as potent methionine aminopeptidase type II inhibitors with antiproliferative properties. *Bioorg. Med. Chem. Lett.* **2006**, *16* (13), 3574–3577.
- (6) Ye, Q.-Z.; Xie, S.-X.; Ma, Z.-Q.; Huang, M.; Hanzlik, R. P. Structural basis for catalysis by monometalated methionine aminopeptidase. *Proc. Natl. Acad. Sci. U.S.A.* **2006**, *103* (25), 9470–9475.
- (7) (a) Schroder, J.; Henke, A.; Wenzel, H.; Brandstetter, H.; Stammer, H. G.; Stammer, A.; Pfeiffer, W. D.; Tschesche, H. Structure-based design and synthesis of potent matrix metalloproteinase inhibitors derived from 6H-1,3,4-thiadiazine scaffold. *J. Med. Chem.* **2001**, *44*, 3231–3243. (b) Auge, F.; Hornebeck, W.; Decarme, M.; Laronze, J.-Y. Improved gelatinase A selectivity by novel zinc binding groups containing galardin derivatives. *Bioorg. Med. Chem. Lett.* **2003**, *13*, 1783–1786. (c) Wang, J.; Sheppard, G. S.; Lou, P.; Kawai, M.; Park, C.; Egan, D.; Schneider, A.; Bouska, J.; Lesniewski, R.; Henkin, J. Physiologically relevant metal cofactor for methionine aminopeptidase-2 is manganese. *Biochemistry* **2003**, *42* (17), 5035–5042. (d) Oefner, C.; Douangamath, A.; D'Arcy, A.; Hafeli, S.; Mareque, D.; Sweeney, A. M.; Padilla, J.; Pierau, S.; Schulz, H.; Thormann, M.; Wadman, S.; Dale, G. E. The 1.15 Ångström crystal structure of the *Staphylococcus aureus* methionyl-aminopeptidase and complexes with triazole-based inhibitors. *J. Mol. Biol.* **2003**, *332*, 13–21. (e) Garrabrant, T.; Tuman, R. W.; Ludovici, D.; Tominovich, R.; Simoneax, R. L.; Galemno, R. A.; Johnson, D. L. Small molecule inhibitors of methionine aminopeptidase type 2 (MetAP-2). *Angiogenesis* **2004**, *7* (2), 91–96. (f) Kallander, L. S.; Lu, Q.; Chen, W.; Tomaszek, T.; Yang, G.; Tew, D.; Meek, T. D.; Hofmann, G. A.; Schulz-Pritchard, C. K.; Smith, W. W.; Janson, C. A.; Ryan, M. D.; Zhang, G.-F.; Johanson, K. O.; Kirkpatrick, R. B.; Ho, T. F.; Fisher, P. W.; Mattern, M. R.; Johnson, R. K.; Hansbury, M. J.; Winker, J. D.; Ward, K. W.; Veber, D. F.; Thompson, S. K. 4-Aryl-1,2,3-triazole: A novel template for a reversible methionine aminopeptidase 2 inhibitor, optimized to inhibit angiogenesis *in vivo*. *J. Med. Chem.* **2005**, *48* (18), 5644–5647.
- (8) Kurzer, F.; Douraghi-Zadeh, K. Heterocyclic compounds from urea derivatives. VI. Synthesis and cyclization of 1-amino-3-(*N,N'*-diarylamidino)guanidines and some analogs. *J. Chem. Soc. C* **1965**, 932–937.
- (9) Davidson, J. S. Action of hydrazine hydrate on isodithiobiurets. *J. Chem. Soc. C* **1967**, 2471–2472.
- (10) Joshua, C. P.; Presannan, E.; Thomas, S. K. A one-step synthesis of 1,5-disubstituted 2,4-dithiobiurets and their oxidation to 3,5-disubstituted imino-1,2,4-dithiazolidines. *Indian J. Chem., Sect. B* **1982**, *21* (7), 649–651.
- (11) (a) Whitten, J. P.; Matthews, D. P.; McCarthy, J. R. [2-(Trimethylsilyloxy)methyl (SEM) as a novel and effective imidazole and fused aromatic imidazole protecting group. *J. Org. Chem.* **1986**, *51* (10), 1891–1894. (b) Lipshutz, B. H.; Huff, B.; Hagen, W. Metalations of imidazoles. (Poly)functionalization and conversions to imidazolones. *Tetrahedron Lett.* **1988**, *29* (28), 3411–3414.
- (12) Bell, A. S.; Roberts, D. A.; Ruddock, K. S. A synthesis of 2- and 4(5)-(2-pyridinyl)imidazoles by palladium-catalyzed cross-coupling reactions. *Tetrahedron Lett.* **1988**, *29* (39), 5013–5016.
- (13) (a) Liu, S.; Widom, J.; Kemp, C. W.; Crews, C. M.; Clardy, J. Structure of human methionine aminopeptidase-2 complexed with fumagillin. *Science* **1998**, *282*, 1324–1327. (b) Lowther, W. T.; Orville, A. M.; Madden, D. T.; Lim, S.; Rich, D. H.; Matthews, B. W. *Escherichia coli* methionine aminopeptidase: Implications of crystallographic analyses of the native, mutant, and inhibited enzymes for the mechanism of catalysis. *Biochemistry* **1999**, *38*, 7678–7688.
- (14) Scudiero, D. A.; Shoemaker, R. H.; Paull, K. D.; Monks, A.; Tierney, S.; Nofziger, T. H.; Currens, M. J.; Seniff, D.; Boyd, M. R. Evaluation of a soluble tetrazolium/formazan assay for cell growth and drug sensitivity in culture using human and other tumor cell lines. *Cancer Res.* **1988**, *48* (17), 4827–4833.
- (15) Walker, K. W.; Bradshaw, R. A. Yeast methionine aminopeptidase 1 can utilize either Zn<sup>2+</sup> or Co<sup>2+</sup> as a cofactor: A case of mistaken identity? *Protein Sci.* **1998**, *7*, 2684–2687.
- (16) (a) Gho, Y. S.; Kleinman, H. K.; Sosne, G. Angiogenic activity of human soluble intercellular adhesion molecule-1. *Cancer Res.* **1999**, *59* (20), 5128–5132. (b) Ponce, M. L.; Nomizu, M.; Delgado, M. C.; Kuratomi, Y.; Hoffman, M. P.; Powell, S.; Yamada, Y.; Kleinman, H. K.; Malinda, K. M. Identification of endothelial cell binding sites on the laminin  $\gamma 1$  chain. *Circ. Res.* **1999**, *84* (6), 688–694.
- (17) (a) Cleland, W. W. The kinetics of enzyme-catalyzed reactions with two or more substrates or products. I. Nomenclature and rate equations. *Biochim. Biophys. Acta* **1963**, *67*, 104–137. (b) Cleland, W. W. The kinetics of enzyme-catalyzed reactions with two or more substrates or products. II. Inhibition—nomenclature and theory. *Biochim. Biophys. Acta* **1963**, *67*, 173–187. (c) Cleland, W. W. The kinetics of enzyme-catalyzed reactions with two or more substrates or products. III. Prediction of initial velocity and inhibition patterns by inspection. *Biochim. Biophys. Acta* **1963**, *67*, 188–196.